

Article

Ambivalent Role of Annealing in Tensile Properties of Step-Rolled Ti-6Al-4V with Ultrafine-Grained Structure

Geonhyeong Kim ¹, Taekyung Lee ^{2,*} , Yongmoon Lee ³, Jae Nam Kim ¹, Seong Woo Choi ⁴, Jae Keun Hong ⁴ and Chong Soo Lee ^{1,*} 

¹ Graduate Institute of Ferrous Technology (GIFT), Pohang University of Science and Technology (POSTECH), Pohang 37673, Korea; kkh285@postech.ac.kr (G.K.); jnkims@postech.ac.kr (J.N.K.)

² School of Mechanical Engineering, Pusan National University, Busan 46241, Korea

³ Center for Advanced Aerospace Materials, Pohang University of Science and Technology (POSTECH), Pohang 37673, Korea; ymlee0725@postech.ac.kr

⁴ Advanced Metals Division, Korea Institute of Materials Science, Changwon 51508, Korea; rhkdgh@kims.re.kr (S.W.C.); jkhong@kims.re.kr (J.K.H.)

* Correspondence: taeklee@pnu.ac.kr (T.L.); cslee@postech.ac.kr (C.S.L.); Tel.: +82-51-510-2985 (T.L.); +82-54-279-9009 (C.S.L.)

Received: 23 April 2020; Accepted: 21 May 2020; Published: 22 May 2020



Abstract: Step rolling can be used to mass-produce ultrafine-grained (UFG) Ti-6Al-4V sheets. This study clarified the effect of subsequent annealing on the tensile properties of step-rolled Ti-6Al-4V at room temperature (RT) and elevated temperature. The step-rolled alloy retained its UFG structure after subsequent annealing at 500–600 °C. The RT ductility of the step-rolled alloy increased regardless of annealing temperature, but strengthening was only attained by annealing at 500 °C. In contrast, subsequent annealing rarely improved the elevated-temperature tensile properties. The step-rolled Ti-6Al-4V alloy without the annealing showed the highest elongation to failure of 960% at 700 °C and a strain rate of 10^{-3} s^{-1} . The ambivalent effect of annealing on RT and elevated-temperature tensile properties is a result of microstructural features, such as dislocation tangles, subgrains, phases, and continuous dynamic recrystallization.

Keywords: Ti-6Al-4V; step rolling; grain refinement; superplasticity; continuous dynamic recrystallization

1. Introduction

Ti-6Al-4V alloy is widely used in aerospace industries due to its high specific strength, excellent corrosion resistance, and high service temperature [1]. This alloy also has superior superplasticity and consequent high formability. Accordingly, many complicated aircraft structures are manufactured from Ti-6Al-4V alloys, using superplastic forming to reduce the material's weight for cost saving [2]. This process is typically performed at relatively high temperatures of over 850 °C and low strain rates of less than 10^{-3} s^{-1} ; these processes are expensive, so they increase production cost. Thus, research has been conducted to find ways to reduce the temperature or increase the strain rate (or both) at which superplastic forming is conducted. Grain refinement may be a solution to this challenge [3,4].

An increased fraction of grain boundaries assists grain-boundary sliding (GBS), which is the main mechanism of superplasticity. GBS by dislocation processes or diffusional flow can accommodate a large amount of deformation. Grain refinement can shift region II (i.e., the region of the highest strain rate sensitivity) to faster strain rates [5]. Therefore, grain refinement can achieve superplasticity at low temperatures or fast strain rates or both. Grain size has been reduced using a variety of severe

plastic deformation (SPD) processes, such as equal-channel angular pressing (ECAP) [6], high-pressure torsion (HPT) [7], and multiaxial forging [8]. The grains of Ti-6Al-4V alloy have been reduced to a size of $\sim 0.4 \mu\text{m}$, which has enabled superplasticity at $550 \text{ }^\circ\text{C}$ and a strain rate of $2 \times 10^{-4} \text{ s}^{-1}$ [4]. However, SPD cannot easily produce an appreciable size of product, so the method is not useful for industrial production. Multi-pass caliber rolling has been proposed as a solution [9–11] but is only applicable to fabricating metallic rods rather than plates.

Step rolling [12] has been developed as a grain-refining process to fabricate relatively large Ti plates. This method can fabricate ultrafine-grained (UFG) bulk Ti-6Al-4V plate (i.e., $300 \text{ mm} \times 70 \text{ mm} \times 4 \text{ mm}$, with grain size $d = 0.5 \mu\text{m}$) with only a small cumulative strain of 1.6. Step rolling is performed by decreasing the rolling temperature step by step. Initial deformation is imposed at a high temperature to effectively fragment the martensitic laths. This fragmentation increases the formability of the material so that the plate can be rolled at progressively lower temperatures in subsequent rolling passes. This low-temperature rolling suppresses grain growth and thereby achieves significant grain refinement with a relatively low amount of plastic strain [12].

The superplasticity of Ti-6Al-4V obtained by step rolling and subsequent annealing was recently reported [13], but the study used only one deformation condition (i.e., a deformation temperature of $750 \text{ }^\circ\text{C}$ and a strain rate of 10^{-3} s^{-1}). However, superplastic behavior drastically varies with deformation temperature and $\dot{\epsilon}$, so to exploit the advantage of step rolling, the high-temperature deformation behavior must be quantified at a wide range of these parameters. Therefore, the present study is a systematic investigation of the deformation behavior of step-rolled Ti-6Al-4V alloys at room temperature (RT) and elevated temperatures under a range of $\dot{\epsilon}$.

2. Materials and Methods

The Ti-6Al-4V alloy used in this study (supplied by ATI, USA) was a 20 mm-thick plate with a chemical composition (mass %) of 6.28 Al, 4.00 V, 0.18 Fe, 0.178 O, and 0.012 C, in balance with Ti. Thermomechanical processing was achieved using step rolling (Figure 1). The as-received plate was solution-treated at $1050 \text{ }^\circ\text{C}$ for 30 min, then quenched in water to induce the formation of a full martensitic structure. The plate was soaked at $800 \text{ }^\circ\text{C}$ for 1 h, then step-rolled to a thickness of 3 mm. The step rolling was composed of eight passes with decreasing temperatures: $800 \text{ }^\circ\text{C}$ for the first pass, $725 \text{ }^\circ\text{C}$ for the second and third passes, and $650 \text{ }^\circ\text{C}$ for the fourth to eighth passes. The sample was then cooled in air to RT. The step-rolled sample without additional heat treatment is denoted as STEP-0. Sections of the STEP-0 sample were further annealed at $500 \text{ }^\circ\text{C}$ (sample STEP-5) or $600 \text{ }^\circ\text{C}$ (STEP-6) for 150 min in an electric furnace (AWF13, Lenton, Hope Valley, UK), then cooled in air to RT.

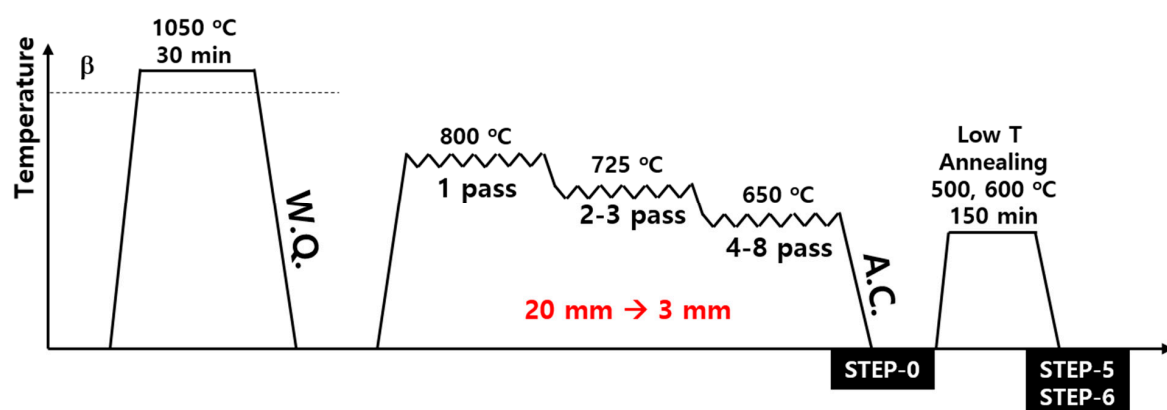


Figure 1. Schematic illustration of the step rolling and subsequent annealing employed in this work.

An RT tensile test was performed at a strain rate of $5 \times 10^{-3} \text{ s}^{-1}$ using a universal mechanical testing machine (8801, INSTRON, Norwood, MA, USA) with an extensometer (3542-025M-100-ST, Epsilon, Jackson, WY, USA), based on the procedure of the ASTM-E8 standard. Plate-type tensile

specimens with a gage length of 25 mm, width of 6 mm, and thickness of 3 mm were machined along the rolling direction. An elevated-temperature tensile test was performed using a universal mechanical testing machine (8862, INSTRON, Norwood, MA, USA) attached to a halogen furnace (DF-60HG, Dae Heung Scientific Company, Incheon, Korea). For this experiment, specimens were prepared with a gauge length of 5 mm, width of 5 mm, and thickness of 2 mm. The elevated-temperature tensile tests were performed at all combinations of the three temperatures (650 °C, 700 °C, 750 °C) and the three initial strain rates (10^{-2} s^{-1} , 10^{-3} s^{-1} , $2 \times 10^{-4} \text{ s}^{-1}$). Samples were held at a given testing temperature for 10 min before the tensile test was started.

For microstructural observation, samples were electro-polished (LectroPol-5, STRUERS, Denmark) in a solution of 410 mL of methanol, 245 mL of 2-butoxy ethyl alcohol, and 40 mL of HClO_4 at 22 V for 30 s. The plane normal to the transverse direction was examined using electron backscatter diffraction (EBSD, FEI QUANTA 3D FEG, Hillsboro, OR, USA) analysis with a step size of 0.1 μm . Quantitative microstructural characterizations were obtained using TSL-OIM Ver. 7.3 software (EDAX, Mahwah, NJ, USA); for data reliability, the scans were only analyzed for points that had a confidence index > 0.07 . More than 1000 validated grains per condition were used for the analysis to ensure statistical accuracy. For examination with transmission electron microscope (TEM, JEM-2100F, JEOL, Tokyo, Japan) observation, the samples were mechanically polished to a thickness $< 100 \mu\text{m}$ and then punched to form thin disks that had a diameter of 3 mm. They were electro-polished using a jet polisher (TenuPol-5, STRUERS, Denmark) at 22 V in the same solution used for the preparation of the EBSD samples.

3. Results and Discussion

3.1. Deformation Behavior at Room Temperature

The microstructures of the step-rolled alloy (i.e., STEP-0) and the subsequently annealed alloys (i.e., STEP-5 and STEP-6) were compared by EBSD analysis (Figure 2). The annealing had little effect on grain size: STEP-0 had a UFG structure with α -grain size $d = 0.70 \mu\text{m}$, STEP-5 had $d = 0.72 \mu\text{m}$, and STEP-6 had $d = 0.74 \mu\text{m}$. This small change implies that annealing induced recovery rather than recrystallization. In contrast, annealing significantly decreased the volume fraction of the β phase: STEP-0, 6.2%; STEP-5, 3.0%; STEP-6, 3.6%.

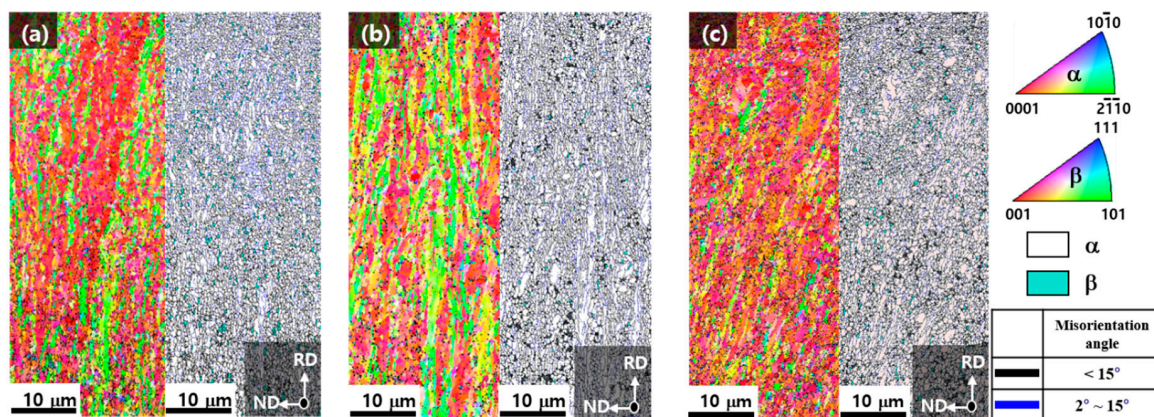


Figure 2. Electron backscatter diffraction (EBSD) inverse pole figure map and corresponding phase map of the samples: (a) STEP-0, (b) STEP-5, (c) STEP-6.

The subsequent annealing caused a marked difference in the RT tensile properties of the samples (Figure 3, Table 1). The STEP-0 sample had an increased yield strength (YS) and ultimate tensile strength (UTS) which were both 20% higher than those of conventional mill-annealed Ti-6Al-4V alloy, which has $d = 10 \mu\text{m}$ [14]. However, STEP-0 showed a decrease in elongation to failure (EL) compared

to the conventional sample [14]. The subsequent annealing of STEP-0 recovered the low EL without loss of mechanical strength.

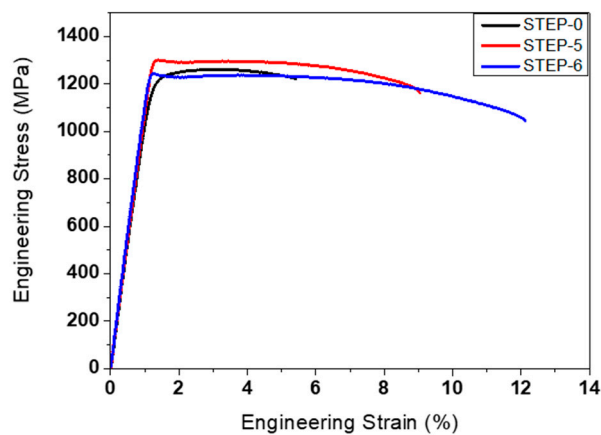


Figure 3. Engineering stress–strain curves of the investigated Ti-6Al-4V alloys at room temperature.

Table 1. Room-temperature tensile properties of the investigated Ti-6Al-4V alloys.

Sample	Yield Strength (YS) (MPa)	Ultimate Tensile Strength (UTS) (MPa)	Elongation to Failure (EL) (%)
STEP-0	1201	1263	5.4
STEP-5	1298	1311	9.0
STEP-6	1243	1243	12.1

Annealing temperature affected the change in strength and ductility differently in each sample. STEP-5 showed an increase in both whereas STEP-6 did not. TEM observation provided a rationalization for the simultaneous improvement in strength and ductility in STEP-5. The TEM micrograph (Figure 4) of STEP-0 showed the formation of dislocation tangles at the grain boundaries (Figure 4a, arrows). Annealing at 500 °C significantly diminished the frequency of dislocation tangles and decreased the dislocation density, resulting in the increased EL. STEP-5 showed fine (i.e., 100–200 nm in diameter) particles; a uniform distribution of fine particles effectively strengthens the matrix [15,16], so they may be the source of the increases in YS and EL in this sample. The selected-area diffraction pattern (Figure 4b, inset) characterizes these particles as α phase. In contrast, the STEP-6 sample showed no evidence of such fine particles. The α particles may have transformed to β phase at this annealing temperature. The absence of fine particles led to the loss of strengthening in STEP-6, compared to STEP-5.

Subsequent annealing affected the substructure of the UFG grains. STEP-0 showed only distributed dislocations (Figure 4c), whereas STEP-5 presented numerous subgrains with diameters of 20–50 nm (Figure 4d). At 500 °C, dislocations at grain boundaries were recovered and organized into subgrains inside a UFG α grain [17]. The consequent increase in the fraction of low-angle grain boundaries (LABs) would also contribute to the increased mechanical strength [18].

3.2. Deformation Behavior at Elevated Temperatures

EL at elevated temperatures was affected by strain rate, deformation temperature, and type of sample (Figure 5). ELs measured at a deformation temperature of 750 °C and $2 \times 10^{-4} \text{ s}^{-1}$ are not presented, because severe oxidation at the sample surface caused large variability in the measurements. An EL of 400% is regarded as the minimum requirement for superplasticity in metals [19]. The investigated alloys exhibited a significant EL of over 400% under most conditions, except at the lowest deformation temperature (650 °C) and the highest strain rate (10^{-2} s^{-1}). The subsequent annealing had an ambivalent effect on the difference between the mechanical properties at RT and those at elevated temperatures:

it rarely increased EL in the step-rolled alloys at elevated temperatures, and it even degraded the ductility at 650 °C.

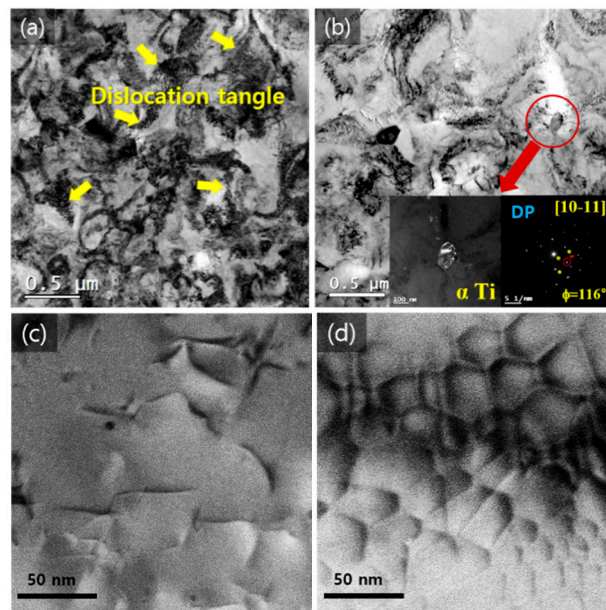


Figure 4. Bright-field transmission electron microscope (TEM) micrographs of (a,c) STEP-0 and (b,d) STEP-5. Insets in (b): dark-field image of α particle and corresponding selected-area diffraction pattern. Figure 4c,d are high-magnification images.

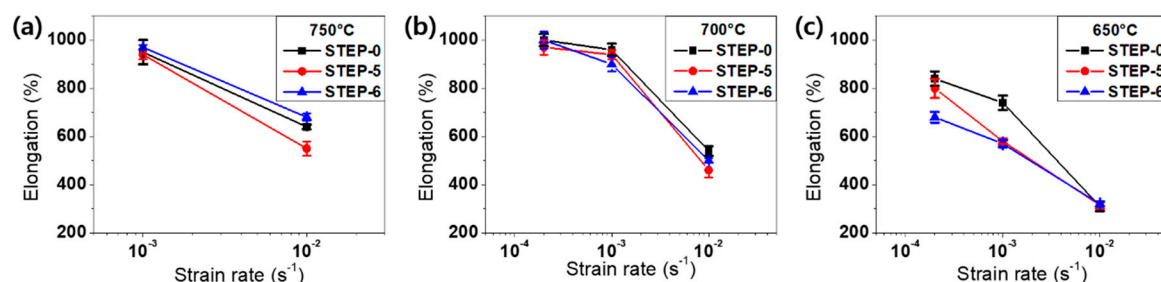


Figure 5. Variation of EL depending on the strain rate for the investigated alloys at (a) 750 °C, (b) 700 °C, and (c) 650 °C.

The stress–strain curves of STEP-0, STEP-5, and STEP-6 were affected by the deformation temperature and strain rate (Figure 6). At 750 °C and 10^{-3} s^{-1} , three specimens showed weak flow hardening behavior. This suggests that continuous dynamic recrystallization (CDRX) could not suppress grain growth, thereby diminishing the superplasticity [20]. The plateau region was confirmed during the deformation at 700 °C, indicating that CDRX strongly suppressed grain growth [21]. To obtain the highest and most efficient superplasticity, this plateau behavior should be achieved. Usually, EL is higher at 750 °C than at 700 °C, but in our results the ELs were similar. In this case, severe grain growth and oxidation degraded the superplasticity at 750 °C. At a deformation temperature of 650 °C, the specimens presented a flow softening followed by the plateau region. Despite the decreasing deformation temperature, they still exhibited significant EL values, suggestive of a low-temperature superplasticity.

The highest superplastic EL of STEP-0 among the investigated step-rolled alloys can be understood in terms of slope m (i.e., strain-rate sensitivity) in a log-scale plot of stress and strain rate (Figure 7). In general, UFG Ti-6Al-4V alloy demonstrates three regions with different slopes in this plot [6,22]. Among them, region II is characterized by (i) an intermediate $10^{-4} \text{ s}^{-1} \leq \dot{\epsilon} \leq 2 \times 10^{-3} \text{ s}^{-1}$, (ii) high m , and (iii) significant superplastic EL. The high m of the STEP-0 sample indicates inhibition of the

transition from region II to region III at a high strain rate of 10^{-2} s^{-1} [23], supporting a superplasticity obtained by the step rolling. Accordingly, the STEP-0 sample had a uniformly high m in the entire range of investigation employed in this work: $m = 0.34$ at $650 \text{ }^\circ\text{C}$, 0.40 at $700 \text{ }^\circ\text{C}$, and 0.55 at $750 \text{ }^\circ\text{C}$. These m are comparable to or higher than those of UFG Ti-6Al-4V alloys fabricated by SPD processes: $0.34 \leq \dot{\epsilon} \leq 0.43$ [4,6,7].

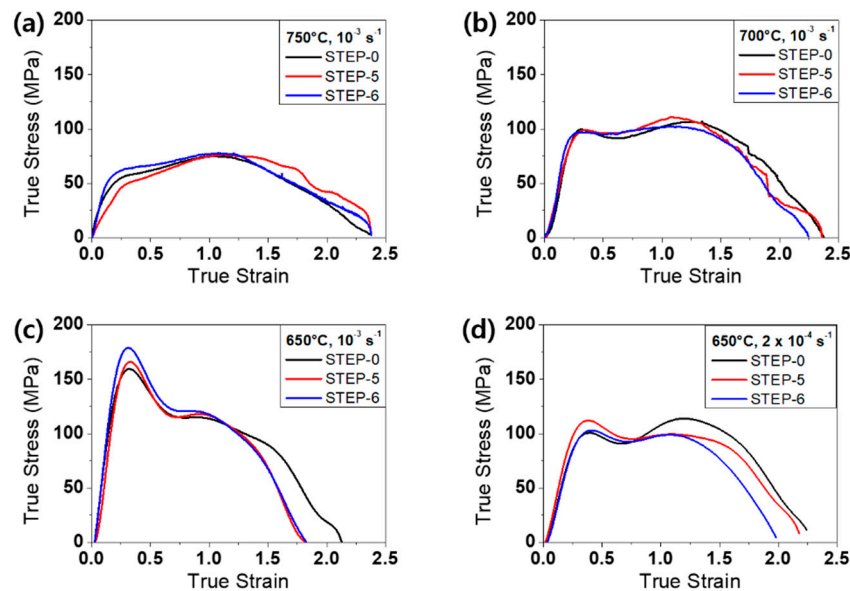


Figure 6. True stress–strain curves of the investigated Ti-6Al-4V alloys at (a) $750 \text{ }^\circ\text{C}$ and strain rate of 10^{-3} s^{-1} , (b) $700 \text{ }^\circ\text{C}$ and 10^{-3} s^{-1} , (c) $650 \text{ }^\circ\text{C}$ and 10^{-3} s^{-1} , and (d) $650 \text{ }^\circ\text{C}$ and $2 \times 10^{-4} \text{ s}^{-1}$.

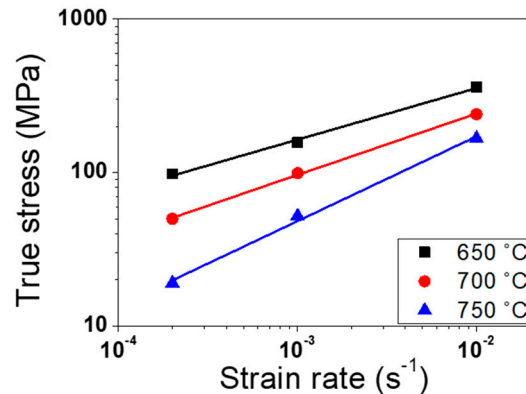


Figure 7. Variation of flow stress as a function of strain rate for STEP-0 specimens.

Step-rolled UFG Ti-6Al-4V yielded excellent superplasticity (i.e., EL up to 960%) that is comparable to the EL obtained using other fabrication methods. ECAP yielded UFG Ti-6Al-4V that had $d = 0.3 \text{ }\mu\text{m}$, EL = 356% at $700 \text{ }^\circ\text{C}$, and 10^{-3} s^{-1} [6]. HPT produced Ti-6Al-4V alloy that had $d \sim 0.03 \text{ }\mu\text{m}$ and EL = 820% under the same conditions [7]. Another HPT study produced $d = 0.3 \text{ }\mu\text{m}$ and the sample had EL = 676% at $725 \text{ }^\circ\text{C}$ and 10^{-3} s^{-1} [24]. Another UFG Ti-6Al-4V alloy ($d = 0.4 \text{ }\mu\text{m}$) produced by hot rolling had EL = 400% at $700 \text{ }^\circ\text{C}$ and 10^{-3} s^{-1} [20]. A combination of forging and warm rolling refined the grains to $d = 0.3 \text{ }\mu\text{m}$; the sample had EL = 550–900% at $700 \text{ }^\circ\text{C}$ [25].

Superplasticity is highly dependent on microstructural features. Grain refinement is regarded as the most important factor to activate superplastic behavior. Grain refinement expands the superplastic regime to lower temperatures and higher $\dot{\epsilon}$, because the increasing fraction of grain boundaries provides increasing sources for GBS [5,9]. Grain morphology also affects superplasticity. Equiaxed grains yield a higher superplastic EL than elongated grains [26,27]. Dislocations distributed at grain boundaries also contribute to superplasticity by providing a fast diffusion path at high temperatures and by increasing

the grain-boundary diffusion coefficient [28]. All of these microstructural features that are beneficial to superplasticity appeared in STEP-0, so its significant EL at 650–750 °C is understandable.

Comparison of the microstructural features at strains of $\varepsilon = 0\%$, 100%, and 300% provided insight into the microstructural evolution during superplastic deformation at elevated temperatures (Figure 8). STEP-0 and STEP-6 were selected for this comparison, because STEP-6 was expected to show more distinct changes in microstructure than STEP-5 due to the higher annealing temperature of STEP-6. In the EBSD map, the STEP-0 and STEP-6 samples showed similar grain sizes before the deformation, whereas the former exhibited a smaller grain size after applying strains of 100% and 300%.

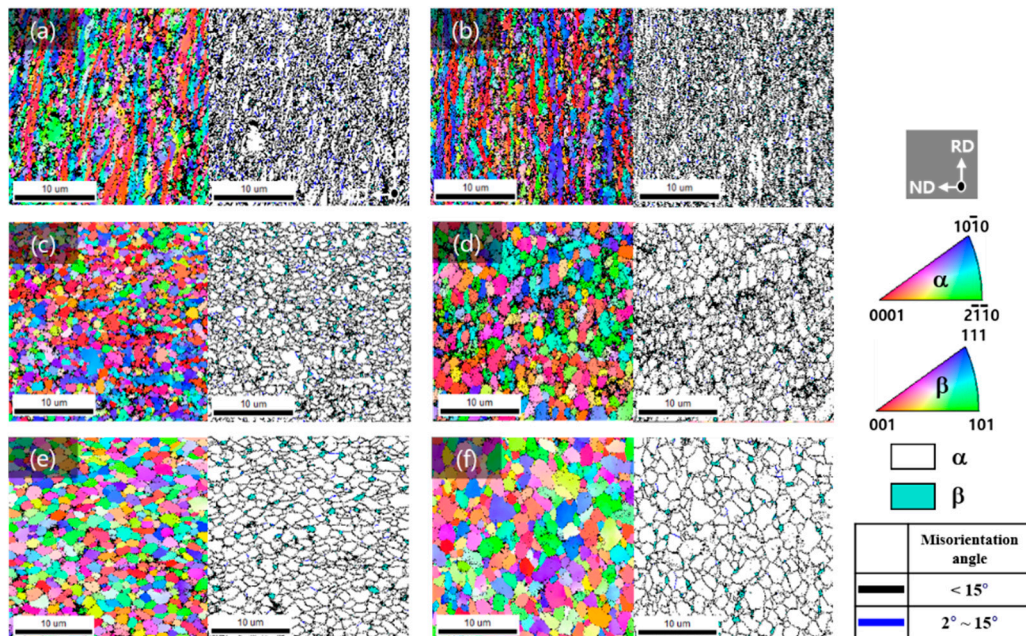


Figure 8. EBSD inverse pole figure maps and phase maps for (a,c,e) STEP-0 and (b,d,f) STEP-6. The micrographs were obtained after a strain of (a,b) 0%, (c,d) 100%, and (e,f) 300%.

Application of ε affected LAB fraction and grain size differently in the two samples (Figure 9). During the early stage of deformation, up to a 100% strain, the LAB fraction was considerably reduced, by 12.2%, in the STEP-0 sample but only by 6.1% in the STEP-6 sample. During this stage, grain size in the STEP-0 sample also increased by only 0.16 μm , whereas in the STEP-6 sample grain size increased by 0.68 μm . Moving from a 100% to a 300% strain, STEP-0 and STEP-6 exhibited a similar reduction in LAB fraction (5.6%) as well as a similar increase in grain size (0.46 μm).

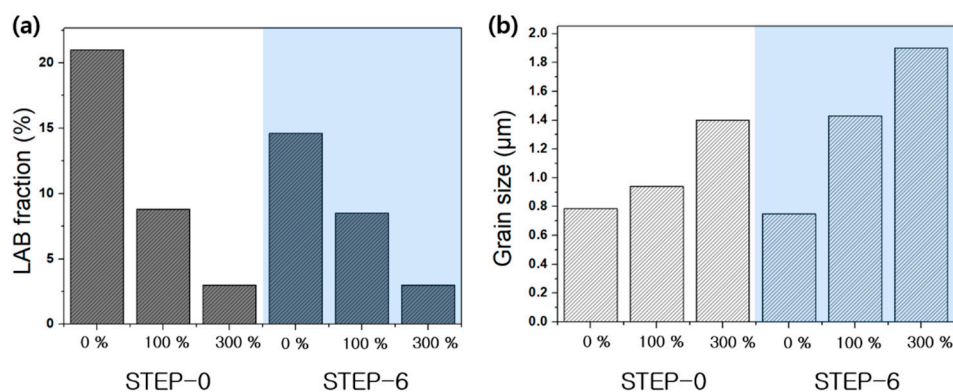


Figure 9. Microstructural features of STEP-0 and STEP-6 samples after strains of 0%, 100%, and 300% at 650 °C and 10^{-3} s^{-1} : (a) LAB fraction, (b) average grain size.

The distinct difference between the microstructural features of STEP-0 and those of STEP-6 arose from the active occurrence of CDRX in the STEP-0 sample. A continuous accumulation of dislocations during high-temperature deformation drove the formation of subgrains surrounded by LAB. Further straining generated recrystallized grains by increasing the misorientation of the subgrain boundaries [17,29]. The higher amount of pre-existing LAB in STEP-0 than in STEP-6 provided a higher driving force for CDRX in comparison with the annealed samples. This result suggests that CDRX of the STEP-0 sample occurred actively during the early stage of deformation, up to a 100% strain.

The hypothesis of the active occurrence of CDRX in STEP-0 during superplastic deformation is supported by the distribution of grain sizes (Figure 10). The STEP-0 sample showed an increasing fraction of grains with a size of $\sim 1 \mu\text{m}$ in exchange for a decreasing fraction of coarse grains. In contrast, in the STEP-6 sample, the peak of the distribution curve shifted towards a higher grain size after a 100% strain at $650 \text{ }^\circ\text{C}$ and 10^{-3} s^{-1} . This is the typical trend that results from dominant grain-growth behavior at an elevated temperature. Such results suggest that the conversion of coarse grains into several fine grains (i.e., CDRX), occurred more actively in STEP-0 than in STEP-6. Consequently, active CDRX during the early stage of deformation in STEP-0 suppressed grain growth during elevated-temperature deformation and thereby contributed to its superior superplasticity.

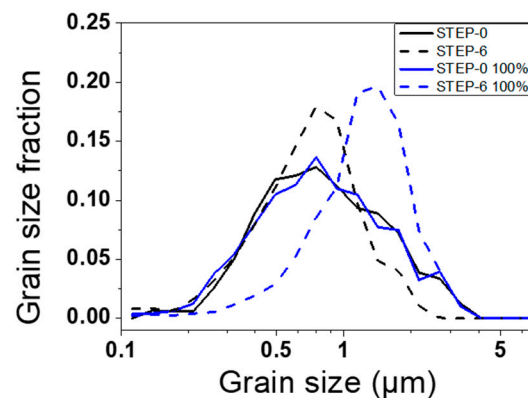


Figure 10. Distribution of grain sizes in STEP-0 and STEP-6 samples before and after applying a strain of 100% at $650 \text{ }^\circ\text{C}$ and 10^{-3} s^{-1} .

β particles also assisted in the increase in superplasticity in the STEP-0 sample. The sample possessed twice as much β phase as the STEP-5 and STEP-6 samples. Due to the difference in their crystallographic structures, grain-boundary diffusivity is over 100 times higher in the β phase than in the α phase [30]. Such a high diffusivity reduces the resistance to GBS activation. Moreover, resistance to GBS is lower at α/β interfaces than at α/α and α/β interfaces [31]. Therefore, the high β fraction was the secondary factor that increased the superplasticity of the STEP-0 sample.

4. Conclusions

This study investigated the RT and elevated-temperature deformation behaviors of UFG Ti-6Al-4V alloys fabricated by step rolling and subsequent annealing. Step rolling attained a significant grain refinement to a size of $0.70 \mu\text{m}$, which was not much changed by subsequent annealing. The STEP-5 sample had significantly increased strength and ductility at RT. The strengthening was a result of the formation of fine α particles and (sub)grains, whereas the increased ductility was the consequence of a decreased frequency of dislocation tangles. The STEP-6 sample lost its strengthening effect because the fine particles disappeared. The STEP-0 sample had the highest superplasticity among the investigated samples; this result suggests that subsequent annealing has a variable influence that depends on the deformation temperature. The superplasticity arose from the equiaxed UFG structure and high dislocation density. Compared to the annealed samples, STEP-0 showed a rapid decrease in LAB fraction during the early stage of deformation. This result suggests that CDRX occurred actively in

the STEP-0 sample at this stage and effectively suppressed grain growth during elevated-temperature deformation. The high β fraction of the STEP-0 sample also contributed to the GBS activation due to the considerable grain-boundary diffusivity and the presence of the α/β interface. Overall, active CDRX and a high content of β particles increased the superplasticity of the STEP-0 sample.

Author Contributions: Conceptualization, G.K. and C.S.L.; Writing—original draft, G.K., T.L., and Y.L.; Writing—review and editing, T.L. and C.S.L.; Supervision, C.S.L.; Investigation, G.K., Y.L., and J.N.K.; Resources, S.W.C. and J.K.H. All authors have read and agreed to the published version of the manuscript.

Funding: This research was funded by a grant (16-CM-MA-10) from Civil-Military Technology Cooperation Program funded by the Ministry of Trade, Industry and Energy, Korea.

Acknowledgments: The authors gratefully acknowledge the financial supports of the Ministry of Trade, Industry and Energy, Korea for this research.

Conflicts of Interest: The authors declare no conflict of interest.

References

1. Welsch, G. *Materials Properties Handbook: Titanium Alloys*; ASM International: Russell Township, OH, USA, 1993; ISBN 9780871704818.
2. Weisert, E. *Proc. AIME Conference on Superplastic Forming of Structural Alloys*; Paton, N.E., Hamilton, C.H., Eds.; TMS-AIME Publications: Warrendale, PA, USA, 1982.
3. Mishra, R.S.; Stolyarov, V.V.; Echer, C.; Valiev, R.Z.; Mukherjee, A.K. Mechanical behavior and superplasticity of a severe plastic deformation processed nanocrystalline Ti-6Al-4V alloy. *Mater. Sci. Eng. A* **2001**, *298*, 44–50. [[CrossRef](#)]
4. Zherebtsov, S.V.; Kudryavtsev, E.A.; Salishchev, G.A.; Straumal, B.B.; Semiatin, S.L. Microstructure evolution and mechanical behavior of ultrafine Ti6Al4V during low-temperature superplastic deformation. *Acta Mater.* **2016**, *121*, 152–163. [[CrossRef](#)]
5. Edington, J.W.; Melton, K.N.; Cutler, C.P. Superplasticity. *Prog. Mater. Sci.* **1976**, *21*, 61–170. [[CrossRef](#)]
6. Ko, Y.G.; Lee, C.S.; Shin, D.H.; Semiatin, S.L. Low-temperature superplasticity of ultra-fine-grained Ti-6Al-4V processed by equal-channel angular pressing. *Metall. Mater. Trans. A* **2006**, *37*, 381–391. [[CrossRef](#)]
7. Shahmir, H.; Naghdi, F.; Pereira, P.H.R.; Huang, Y.; Langdon, T.G. Factors influencing superplasticity in the Ti-6Al-4V alloy processed by high-pressure torsion. *Mater. Sci. Eng. A* **2018**, *718*, 198–206. [[CrossRef](#)]
8. Zherebtsov, S.; Kudryavtsev, E.; Kostjuchenko, S.; Malysheva, S.; Salishchev, G. Strength and ductility-related properties of ultrafine grained two-phase titanium alloy produced by warm multiaxial forging. *Mater. Sci. Eng. A* **2012**, *536*, 190–196. [[CrossRef](#)]
9. Lee, T.; Shih, D.S.; Lee, Y.; Lee, C.S. Manufacturing Ultrafine-Grained Ti-6Al-4V Bulk Rod Using Multi-Pass Caliber-Rolling. *Metals* **2015**, *5*, 777–789. [[CrossRef](#)]
10. Lee, T.; Park, K.-T.T.; Lee, D.J.; Jeong, J.; Oh, S.H.; Kim, H.S.; Park, C.H.; Lee, C.S. Microstructural evolution and strain-hardening behavior of multi-pass caliber-rolled Ti-13Nb-13Zr. *Mater. Sci. Eng. A* **2015**, *648*, 359–366. [[CrossRef](#)]
11. Lee, T.; Lee, S.; Kim, I.-S.; Moon, Y.H.; Kim, H.S.; Park, C.H. Breaking the limit of Young's modulus in low-cost Ti-Nb-Zr alloy for biomedical implant applications. *J. Alloy. Compd.* **2020**, *828*, 154401. [[CrossRef](#)]
12. Park, C.H.; Kim, J.H.; Yeom, J.-T.T.; Oh, C.-S.S.; Semiatin, S.L.; Lee, C.S. Formation of a submicrocrystalline structure in a two-phase titanium alloy without severe plastic deformation. *Scr. Mater.* **2013**, *68*, 996–999. [[CrossRef](#)]
13. Kim, D.; Won, J.W.; Park, C.H.; Hong, J.K.; Lee, T.; Lee, C.S. Enhancing Superplasticity of Ultrafine-Grained Ti-6Al-4V without Imposing Severe Plastic Deformation. *Adv. Eng. Mater.* **2019**, *21*, 1800115. [[CrossRef](#)]
14. Jeong, D.; Kwon, Y.; Goto, M.; Kim, S. High cycle fatigue and fatigue crack propagation behaviors of β -annealed Ti-6Al-4V alloy. *Int. J. Mech. Mater. Eng.* **2017**, *12*, 1. [[CrossRef](#)]
15. Morita, T.; Hatsuoka, K.; Iizuka, T.; Kawasaki, K. Strengthening of Ti-6Al-4V Alloy by Short-Time Duplex Heat Treatment. *Mater. Trans.* **2005**, *46*, 1681–1686. [[CrossRef](#)]
16. Valiev, R.Z.; Alexandrov, I.V.; Enikeev, N.A.; Murashkin, M.Y.; Semenova, I.P. Towards enhancement of properties of UFG metals and alloys by grain boundary engineering using SPD processing. *Rev. Adv. Mater. Sci.* **2010**, *25*, 1–10.

17. Sakai, T.; Belyakov, A.; Kaibyshev, R.; Miura, H.; Jonas, J.J. Dynamic and post-dynamic recrystallization under hot, cold and severe plastic deformation conditions. *Prog. Mater. Sci.* **2014**, *60*, 130–207. [[CrossRef](#)]
18. Muga, C.O.; Zhang, Z.W. Strengthening Mechanisms of Magnesium-Lithium Based Alloys and Composites. *Adv. Mater. Sci. Eng.* **2016**, *2016*, 1078187. [[CrossRef](#)]
19. Langdon, T.G. Seventy-five years of superplasticity: Historic developments and new opportunities. *J. Mater. Sci.* **2009**, *44*, 5998. [[CrossRef](#)]
20. Matsumoto, H.; Velay, V.; Chiba, A. Flow behavior and microstructure in Ti–6Al–4V alloy with an ultrafine-grained α -single phase microstructure during low-temperature-high-strain-rate superplasticity. *Mater. Des.* **2015**, *66*, 611–617. [[CrossRef](#)]
21. Semiatin, S.L.; Fagin, P.N.; Betten, J.F.; Zane, A.P.; Ghosh, A.K.; Sargent, G.A. Plastic Flow and Microstructure Evolution during Low-Temperature Superplasticity of Ultrafine Ti–6Al–4V Sheet Material. *Metall. Mater. Trans. A* **2010**, *41*, 499–512. [[CrossRef](#)]
22. Alabort, E.; Kontis, P.; Barba, D.; Dragnevski, K.; Reed, R.C. On the mechanisms of superplasticity in Ti–6Al–4V. *Acta Mater.* **2016**, *105*, 449–463. [[CrossRef](#)]
23. Lee, T.; Yamasaki, M.; Kawamura, Y.; Lee, Y.; Lee, C.S. High strain-rate superplasticity of AZ91 alloy achieved by rapidly solidified flaky powder metallurgy. *Mater. Lett.* **2019**, *234*, 245–248. [[CrossRef](#)]
24. Sergueeva, A.V.; Stolyarov, V.V.; Valiev, R.Z.; Mukherjee, A.K. Superplastic behaviour of ultrafine-grained Ti–6Al–4V alloys. *Mater. Sci. Eng. A* **2002**, *323*, 318–325. [[CrossRef](#)]
25. Salishchev, G.A.; Galeyev, R.M.; Valiakhmetov, O.R.; Safiullin, R.V.; Lutfullin, R.Y.; Senkov, O.N.; Froes, F.H.; Kaibyshev, O.A. Development of Ti–6Al–4V sheet with low temperature superplastic properties. *J. Mater. Process. Technol.* **2001**, *116*, 265–268. [[CrossRef](#)]
26. Paton, N.E.; Hamilton, C.H. Microstructural influences on superplasticity in Ti–6Al–4V. *Metall. Trans. A* **1979**, *10*, 241–250. [[CrossRef](#)]
27. Park, C.H.; Ko, Y.G.; Park, J.-W.W.; Lee, C.S. Enhanced superplasticity utilizing dynamic globularization of Ti–6Al–4V alloy. *Mater. Sci. Eng. A* **2008**, *496*, 150–158. [[CrossRef](#)]
28. Ovid'ko, I.A.; Sheinerman, A.G. Grain-boundary dislocations and enhanced diffusion in nanocrystalline bulk materials and films. *Philos. Mag.* **2003**, *83*, 1551–1563. [[CrossRef](#)]
29. Huang, K.; Logé, R.E. A review of dynamic recrystallization phenomena in metallic materials. *Mater. Des.* **2016**, *111*, 548–574. [[CrossRef](#)]
30. Wert, J.A.; Paton, N.E. Enhanced superplasticity and strength in modified Ti–6Al–4V alloys. *Metall. Mater. Trans. A* **1983**, *14*, 2535–2544. [[CrossRef](#)]
31. Kim, J.S.; Chang, Y.W.; Lee, C.S. Quantitative analysis on boundary sliding and its accommodation mode during superplastic deformation of two-phase Ti–6Al–4V alloy. *Metall. Mater. Trans. A* **1998**, *29*, 217–226. [[CrossRef](#)]

